J Math Chem (2010) 47:569–589
DOI 10.1007/s10910-009-9586-5

ORIGINAL PAPER

Silicon nanotubes with distinct bond lengths

Richard K. F. Lee · Barry J. Cox · James M. Hill

Received: 15 April 2009 / Accepted: 10 August 2009 / Published online: 30 August 2009

Abstract In this paper, we extend both the rolled-up and the polyhedral models for single-walled silicon nanotubes with equal bond lengths to models having distinct bond lengths. The silicon nanotubes considered here are assumed to be formed by sp^3 hybridization with different bond lengths so that the nanotube lattice is assumed to comprise only skew rhombi. Beginning with the three postulates that all bonds lying on the same helix are equal, all adjacent bond angles are equal, and all atoms are equidistant from a common axis of symmetry, we derive exact formulae for the polyhedral geometric parameters such as chiral angles, bond angles, radius and unit cell length. The polyhedral model presented here with distinct bond lengths includes both the rolled-up model with distinct bond lengths which arises from the first term of an asymptotic expansion, and an existing polyhedral model of the authors which assumes equal bond lengths. Finally, some molecular dynamics simulations are undertaken for comparison with the geometric model. These simulations start with equal bond lengths and then stabilize in such a way that two distinct bond lengths emerge.

Keywords Silicon nanotubes · Geometry · Polyhedral model · Distinct bond lengths · Molecular dynamics simulations

1 Introduction

Due to silicon's similarity to carbon there is considerable interest in nano-structures, such as nanowires and nanotubes, formed from silicon. Recent interest in carbon

R. K. F. Lee (✉) · B. J. Cox · J. M. Hill
Nanomechanics Group, School of Mathematics and Applied Statistics,
University of Wollongong, Wollongong, NSW 2522, Australia
e-mail: kfrl145@uow.edu.au; richard7li@yahoo.com.hk

B. J. Cox
e-mail: barryc@uow.edu.au

nanotubes was ignited by Iijima's discovery in 1991 [1] and recently silicon nanotubes have been synthesized by both molecular beam epitaxy [2] and physical and chemical vapor deposition [3] and large diameter silicon nanotubes are observed in [3]. Silicon and carbon belong to the same group of the periodic table but silicon and carbon nanotubes have different bond configurations. Carbon nanotubes have a very stable structure formed from sp^2 hybridized bonds [4,5], which leads to carbon nanotubes adopting a hexagonal honeycomb structure. On the other hand, silicon adopts an sp^3 bond structure and therefore the four-coordinated atoms form a quadrilateral lattice [4,6–9].

Most theoretical studies have investigated the structure of nanotubes assuming the conventional rolled-up model for carbon nanotubes [10–12] and boron nanotubes [13,14], where these nanotubes are conceptualized as two dimensional sheets that are then rolled into right circular cylinders. Silicon nanotubes might also be considered to be rolled up from silicon sheets. Recently, Cox and Hill [15,16] propose a new geometric polyhedral model of single-walled carbon nanotubes, in which all bond lengths are assumed to be equal, and which makes predictions on the geometric parameters of the nanotubes which are in excellent agreement with first-principles calculations [15]. The corresponding geometric polyhedral model for silicon with equal bond lengths is formulated by the present authors in [17]. Harmonic vibrational analysis based on Moller–Plesset perturbation theory using a second order level molecular-orbital theory [9] suggests that the bond lengths of silicon nanotubes have different lengths in different directions. For the present work we employ a similar polyhedral model to that formulated in [15,16] for carbon nanotubes and [17] for silicon nanotubes to represent single-walled silicon nanotubes but we extend the model to allow for distinct bond lengths.

The silicon nanotubes considered here are all assumed to comprise a skew rhombic lattice of four coordinated atoms. As detailed in Lee et al. [17], the terminology adopted for carbon nanotubes, namely zigzag and armchair, is entirely inappropriate for silicon nanotubes, and here we follow [17] and categorize these tubes as being either prismatic, antiprismatic or chiral type based on the values of the chiral vector numbers (n, m). When $m = 0$, we refer to these nanotube types as prismatic. In the case $m = n$, we term these nanotubes as antiprismatic. In all other cases, when $0 < m < n$, we follow the carbon nanotube terminology and term the nanotube as chiral.

The geometric polyhedral model for silicon nanotubes with distinct bond lengths is developed in a similar manner to that for the geometric polyhedral model for carbon nanotubes [15,16] and for silicon nanotubes [17] and is based on the following three fundamental postulates: (i) corresponding bonds lying on the same helix are equal in length to either σ_1 or σ_2 which are assumed generally to be distinct; (ii) all adjacent bond angles are equal to ϕ; and (iii) all atomic nuclei are equidistant r from a common axis. Silicon nanotubes generated from this polyhedral model are shown in Fig. 1 with $\sigma_1 = 2.35$ Å and $\sigma_2 = 2.75$ Å. In this figure the silicon atoms are represented by black dots and the bonds between silicon atoms are indicated by black lines.

In Sects. 2 and 3 we extend the rolled-up model and the polyhedral model for silicon nanotubes with distinct bond lengths, respectively. In Sect. 4 we give the asymptotic expansions for the formulae from Sect. 3 including the first two leading order terms.

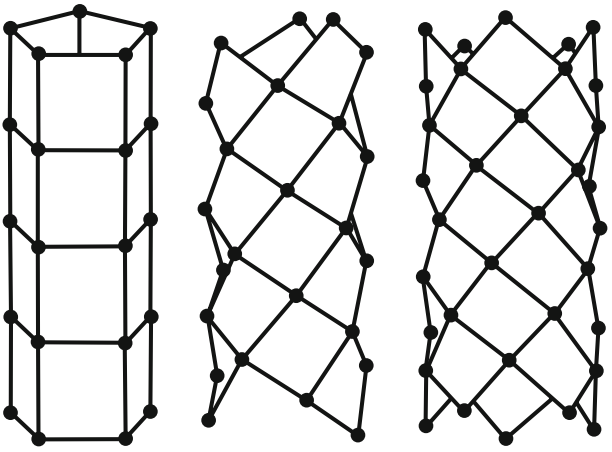

Fig. 1 Polyhedral model for silicon nanotubes for prismatic, chiral and antiprismatic tubes with $\sigma_1 = 2.35$ Å and $\sigma_2 = 2.75$ Å

In Sect. 5 the radius is discussed for different bond lengths and some molecular dynamics simulations are undertaken for comparison with the geometric model. Some concluding remarks are made in the Sect. 6. Appendix A provides details for some of the asymptotic expansions for the main geometric parameters.

2 Rolled-up model with distinct bond lengths for silicon nanotubes

Employing the same concept as that used for carbon nanotubes, we apply the (n, m) naming scheme to identify the specific configuration of the silicon nanotube originating from the rolled-up model [10–14]. From Fig. 2, three different types of silicon nanotubes can be defined by the value of m in relation to n. The naming convention we employ for silicon nanotubes is different to the corresponding convention adopted for hexagonal latices, e.g. carbon nanotubes. This difference is necessary because the conventional terms are not applicable to a skew rhombi geometry. As noted above, when $m = 0$, we term the resulting nanotube to be prismatic. This is equivalent to the direction of rolling up of the nanotube OE and we use this term because the tube comprises regular n-gon prisms. The second type, which we term antiprismatic, occurs when $m = n$. In this case, the sheet is rolled following the direction OD. Chiral tubes arise by rolling in a direction which is between OD and OE. The (n, m) naming scheme for the nanotubes can be thought of as the chiral vector $\mathbf{C_h}$, shown on Fig. 2. In this figure we show a silicon nanotube of type (4, 2). The vector OB is called the conventional translational vector $\mathbf{T_0}$ and consists of the vectors $\mathbf{a_1}$ and $\mathbf{a_2}$ which are divided by the greatest common divisor d_{0R} of n and m, and we have

$$\mathbf{C_h} = n\mathbf{a_1} + m\mathbf{a_2},$$
$$\mathbf{T_0} = -m\mathbf{a_1}/d_{0R} + n\mathbf{a_2}/d_{0R},$$

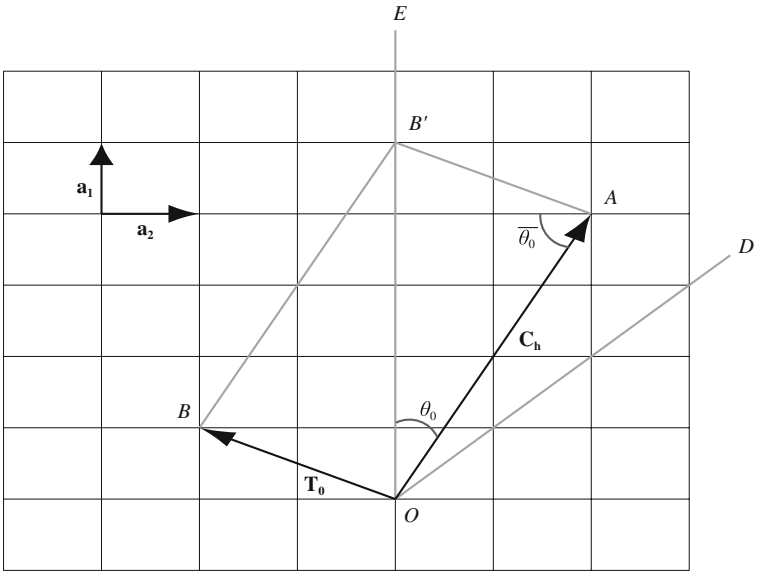

Fig. 2 Silicon nanotube constructed from two dimensional sheet

where n and m are the integers from the (n, m) naming scheme, $\mathbf{a_1}$ and $\mathbf{a_2}$ are basis vectors in real space where $|\mathbf{a_1}| = \sigma_1$ and $|\mathbf{a_2}| = \sigma_2$, where σ_1 and σ_2 are different bond lengths, and d_{0R} is the greatest common divisor of n and m. We note that throughout we use the subscript 0 to designate quantities associated with the conventional rolled-up model.

In Fig. 2 the origin O is located at an arbitrary lattice point. The conventional translational vector $\mathbf{T_0}$ is perpendicular to the chiral vector $\mathbf{C_h}$ when the bond lengths are equal. However, in general they are not perpendicular. The sheet is rolled up to form a nanotube where the point A will coincide with the origin O and the point B will coincide with the point B'. From Fig. 2 the conventional chiral angle θ_0 is found to be

$$\cos^2\theta_0 = \sigma_1^2 n^2 / \left(\sigma_1^2 n^2 + \sigma_2^2 m^2\right). \tag{1}$$

The conjugate chiral angle $\bar{\theta_0}$ which is $90°-\theta_0$ is expressed as

$$\cos^2\bar{\theta_0} = \sigma_2^2 m^2 / \left(\sigma_1^2 n^2 + \sigma_2^2 m^2\right), \tag{2}$$

with the relationship $\cos\bar{\theta_0} = \sin\theta_0$.

Silicon nanotubes are also considered to be constructed from a repeating unit cell, when the ratio of the bond lengths $\lambda^2 = \sigma_1^2/\sigma_2^2 = p_\lambda/q_\lambda$ is rational. In other cases, the nanotubes have no repeating unit cell. The unit cell length for the rolled-up model is not the length of the conventional translational vector $|\mathbf{T_0}|$, since the conventional translational vector $\mathbf{T_0}$ and the chiral vector $\mathbf{C_h}$ are not perpendicular. For bond lengths that are not equal, the new translational vector $\mathbf{T}$ which is perpendicular to the chiral vector $\mathbf{C_h}$ is given by

$$\mathbf{T} = -mq_\lambda \mathbf{a_1}/d_R + np_\lambda \mathbf{a_2}/d_R,$$

where

$$\lambda^2 = \sigma_1^2/\sigma_2^2 = p_\lambda/q_\lambda, \quad d_R = \gcd(np_\lambda, mq_\lambda),$$

where p_λ and q_λ are relatively prime integers and $\gcd(x, y)$ is the greatest common divisor of x and y, and when the bond lengths are equal, the values of p_λ and q_λ are one. The conventional translational vector $\mathbf{T_0}$ is a special case arising from equal bond lengths of the new translational vector $\mathbf{T}$. The unit cell length for the rolled-up model is the length of the new translational vector $|\mathbf{T}|$ which is given by

$$L_0 = \sqrt{\sigma_2^2 n^2 p_\lambda^2 + \sigma_1^2 m^2 q_\lambda^2}/d_R. \tag{3}$$

Prismatic ($m = 0$) and antiprismatic tubes ($m = n$) have exact values for the unit cell length which are $L_0 = \sigma_2$ and $L_0 = n\sqrt{2\sigma_1\sigma_2 p_\lambda q_\lambda}/d_R$, respectively. The number of atoms in a unit cell N is given by $N = |\mathbf{C_h} \times \mathbf{T}|/|\mathbf{a_1} \times \mathbf{a_2}|$ and therefore the number of atoms in the unit cell for the rolled-up model is found to be given by

$$N = (n^2 p_\lambda + m^2 q_\lambda)/d_R. \tag{4}$$

When the bond lengths are equal, the values of the unit cell length and the number of atoms are the same as those given in Lee et al. [17]. The conventional radius equation for the nanotube is given by the magnitude of the chiral vector $|\mathbf{C_h}|$, divided by 2π and thus

$$r_0 = \sqrt{\sigma_1^2 n^2 + \sigma_2^2 m^2}/(2\pi). \tag{5}$$

3 Polyhedral model with distinct bond lengths for silicon nanotubes

The polyhedral model with distinct bond lengths for silicon nanotubes is similar to the ideal polyhedral models for carbon nanotubes [15,16] and for silicon nanotubes [17]. From the fundamental postulate (iii) that all atoms in the silicon nanotube are equidistant from a common axis, it follows that the vertices of each face cannot be coplanar except in the special case of prismatic tubes and therefore in the rolled-up state, the lattice generally comprises skew rhombi. For the ideal polyhedral model of carbon nanotubes, each hexagonal lattice is divided into three isosceles triangles and one equilateral triangle [15,16]. However, as we demonstrate below, the skew rhombic lattice does not need to be subdivided. We begin by defining a cylinder on whole surface is traced out a family of helices that correspond to the lattice lines in the direction of $\mathbf{a_1}$. Therefore, from Fig. 2 it may easily be shown that the number of helices is equivalent to the value of m and the silicon atoms are positioned on these helices where the helices are shown on Fig. 3 which $|\mathbf{PQ}| = \sigma_1$ and $|\mathbf{PR}| = \sigma_2$.

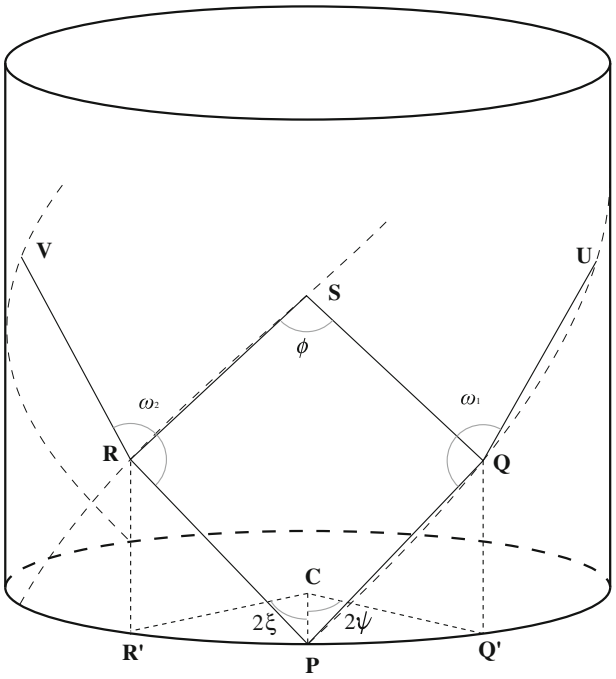

Fig. 3 Points lying on three helices and forming a skew rhombus in three-dimensional space

From postulates (i) and (ii), the fundamental parameter for the polyhedral model with distinct bond lengths is the subtend semi-angle ψ, which is determined from the equation:

$$4nm\left(\sin^2\psi - \lambda^2\sin^2\xi\right) + \left(\lambda^2 n^2 - m^2\right)\left[\sin^2(\xi+\psi) - \sin^2(\xi-\psi)\right] = 0, \quad (6)$$

where $\xi = (n\psi - \pi)/m$ and $\lambda = \sigma_1/\sigma_2$. The subtend semi-angle ψ is determined as the root of this equation. We observe that the root of Eq. 6 depends on the ratio $\lambda = \sigma_1/\sigma_2$ and the values of n and m. Equation 6 may have many roots but based on a specific requirement the subtend semi-angle ψ must also satisfy the following inequalities

$$\begin{cases} \pi/(n+m) \le \psi \le \pi/n & \text{when } \lambda \ge 1, \\ 0 \le \psi \le \pi/n & \text{when } \lambda < 1. \end{cases}$$

The root of Eq. 6 which also satisfies these inequalities can be accurately determined numerically by a small number of iterations of Newton's method, using the initial value of the root given by $\psi_0 = \sigma_1^2 n\pi/(\sigma_1^2 n^2 + \sigma_2^2 m^2)$. From Eq. 6 the exact values of the subtend semi-angle ψ is found as $\psi = \pi/n$ for the prismatic type $m = 0$. From the initial value equation, the subtend semi-angle ψ depends on n, m and a ratio of

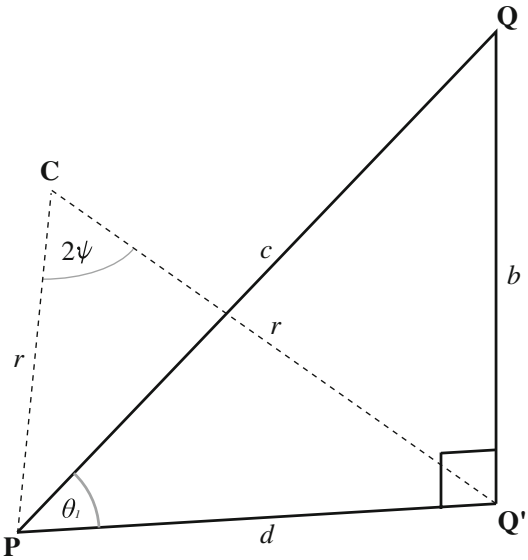

Fig. 4 Points forming **PQQ′** in three-dimensional space

bond lengths λ except prismatic $(n, 0)$ that is not similar to ideal polyhedral model which the subtend semi-angle ψ depends only on n and m.

The true chiral angle θ_1, by which we mean $\angle$**QPQ′**, is found by considering a triangle comprising the points **P**, **Q** and a new point **Q′** which we define as the point determined by projecting **Q** into the xy-plane as shown in the Fig. 4. The conjugate chiral angle θ_2 is the angle of $\angle$**RPR′** where **R′** is the point determined by projecting **R** into the xy-plane as shown in the Fig. 3. Similarly, the conjugate chiral angle θ_2 is found by triangles $\triangle$**PRR′** and $\triangle$**CPR′**. The true chiral angle θ_1 and the conjugate chiral angle θ_2 corresponding to the chiral angle θ_0 and the conjugate chiral angle $\bar{\theta_0}$ are given by

$$\begin{aligned} \cos^2\theta_1 &= (n\sin\psi)/(n\sin\psi - m\cos\psi\sin\xi\cos\xi), \\ \cos^2\theta_2 &= (m\sin\xi)/(m\sin\xi - n\sin\psi\cos\psi\cos\xi). \end{aligned} \tag{7}$$

The adjacent bond angle ϕ is defined as the angle between two bonds where the atoms that are being bonded form part of the same rhombus in the nanotube lattice and an opposite bond angle is the angle between two bonds where the atoms that are being bonded do not form part of the same rhombus in the nanotube lattice. The adjacent bond angle ϕ and the two opposite bond angles ω_1 and ω_2 are derived from the cosine law. The adjacent bond angle is found by considering a triangle comprising the points **R**, **S** and **Q**. Using the same technique, the opposite bond angle ω_1 is found from the triangle $\triangle$**PQU** and the opposite bond angle ω_2 is found from the triangle $\triangle$**PRV**. The adjacent bond angle ϕ is given by

$$\begin{aligned} \cos\phi = [(\lambda^2+1)m^2\sin^2\psi - \lambda^2 m^2\cos^2\theta_1\sin^2(\xi+\psi) \\ -\lambda^2(n+m)^2\sin^2\theta_1\sin^2\psi]/(2\lambda m^2\sin^2\psi), \end{aligned} \tag{8}$$

and the opposite bond angles ω_1 and ω_2 are given by

$$\cos\omega_1 = 2\cos^2\theta_1 \sin^2\psi - 1,$$
$$\cos\omega_2 = 1 - (2\lambda^2 n^2 \sin^2\theta_1)/m^2 - [\lambda^2 \cos^2\theta_1 \sin^2(2\xi)]/(2\sin^2\psi). \quad (9)$$

The nanotube radius r is the distance from each silicon atom to the axis of the nanotube which may be found from $\cos\theta_1$ in Fig. 4 and the length of $|\mathbf{PQ}| = c = \sigma_1$, the length of a silicon-silicon covalent bond, and therefore the nanotube radius r is given by

$$r = (\sigma_1 \cos\theta_1)/(2\sin\psi). \quad (10)$$

Since both θ_1 and ψ depend only on the ratio $\lambda = \sigma_1/\sigma_2$, we observe that the radius r as a function of σ_1 and σ_2 is homogenous of degree one.

Silicon nanotubes might be considered to be constructed from a repeating unit cell, when the ratio of the bond lengths λ is rational. The number of atoms in the unit cell N for the polyhedral model is the same as the rolled-up model, which is the Eq. 4. A unit cell length L is the number of atoms in a single helix multiplied by the helical vertical spacing coefficient b. The number of atoms in a single helix is found from the number of atoms in a unit cell N divided by m helices. Thus for the unit cell length we may derive from $L = Nb/m$ and the expression is

$$L = [\sigma_1(n^2 p_\lambda + m^2 q_\lambda)\sin\theta_1]/(m d_R), \quad (11)$$

where the values of p_λ and q_λ are the same as those for the rolled-up model.

4 Asymptotic expansions for polyhedral model

As shown in Appendix A, the equations of the polyhedral model may be expanded in terms of expansions of n and m in the limit of $n \to \infty$ by using the method of asymptotic expansions. The subtend semi-angle ψ determined from the transcendental Eq. 6 is given by

$$\psi = \frac{\sigma_1^2 n\pi}{\sigma_1^2 n^2 + \sigma_2^2 m^2} - \frac{\sigma_1^2\sigma_2^2 nm^2\pi^3\left[\sigma_1^6 n^4 - 2\sigma_1^2\sigma_2^2 n^2 m^2\left(\sigma_1^2 - \sigma_2^2\right) - \sigma_2^6 m^4\right]}{3\left(\sigma_1^2 n^2 + \sigma_2^2 m^2\right)^5} + O\left(\frac{1}{n^5}\right), \quad (12)$$

where the $O(1/n^5)$ term refers to the maximum order of the magnitude of the next most significant term. The first term of Eq. 12 gives the leading order behavior for the subtend semi-angle ψ and the second term may be viewed as a correction term which takes into account the curvature of the cylinder in question. It is worth commenting that up to this order Eq. 12 is totally in accordance with the special case of prismatic nanotubes $m = 0$, where $\psi = \pi/n$.

By substituting Eq. 12 into the expressions for the true chiral angle θ_1 and the conjugate chiral angle θ_2 given in Eq. 7 and then by further expansion in terms of

$1/n$, an expansion for the true chiral angle θ_1 and the conjugate chiral angle θ_2 may be developed which are given by

$$\cos^2\theta_1 = \frac{\sigma_1^2 n^2}{\sigma_1^2 n^2 + \sigma_2^2 m^2} + \frac{\sigma_1^2\sigma_2^4 n^2 m^4 \pi^2 \left(\sigma_1^4 n^2 + \sigma_2^4 m^2\right)}{\left(\sigma_1^2 n^2 + \sigma_2^2 m^2\right)^5} + O\left(\frac{1}{n^4}\right),$$
$$\cos^2\theta_2 = \frac{\sigma_2^2 m^2}{\sigma_1^2 n^2 + \sigma_2^2 m^2} + \frac{\sigma_1^4\sigma_2^2 n^4 m^2 \pi^2 \left(\sigma_1^4 n^2 + \sigma_2^4 m^2\right)}{\left(\sigma_1^2 n^2 + \sigma_2^2 m^2\right)^5} + O\left(\frac{1}{n^4}\right), \quad (13)$$

where the leading order term is exactly the corresponding angles θ_0 and $\bar{\theta_0}$ which are the conventional expressions of the chiral angle (1) and the conjugate chiral angle (2). The second term is the first-order correction to the conventional chiral angle θ_0 and it may be shown that Eq. 13 can be expressed as

$$\cos^2\theta_1 = \cos^2\theta_0 + \left[\cos^2\theta_0 \sin^4\theta_0 \left(\sigma_1^2 \cos^2\theta_0 + \sigma_2^2 \sin^2\theta_0\right)\right] / \left(4r_0^2\right) + O(1/n^4),$$
$$\cos^2\theta_2 = \cos^2\bar{\theta_0} + \left[\cos^2\bar{\theta_0} \sin^4\bar{\theta_0} \left(\sigma_2^2 \cos^2\bar{\theta_0} + \sigma_1^2 \sin^2\bar{\theta_0}\right)\right] / (4r_0^2) + O(1/n^4), \quad (14)$$

where r_0 is the conventional radius. The asymptotic expansion of the conjugate chiral angle θ_2 might also be expressed as

$$\cos^2\theta_2 = \sin^2\theta_0 + \left[\cos^4\theta_0 \sin^2\theta_0 \left(\sigma_1^2 \cos^2\theta_0 + \sigma_2^2 \sin^2\theta_0\right)\right] / (4r_0^2) + O(1/n^4),$$

since the conventional conjugate chiral angle has a relationship with θ_0 is $\cos\bar{\theta_0} = \sin\theta_0$.

The expansion equation for the adjacent bond angle ϕ is found by substituting Eq. 12 in Eq. 8, where upon the expansion of $\cos\phi$ is given by

$$\cos\phi = \frac{\sigma_1^3\sigma_2^3 n^2 m^2 \pi^2}{\left(\sigma_1^2 n^2 + \sigma_2^2 m^2\right)^3} + \frac{\sigma_1^3\sigma_2^3 n^2 m^2 \pi^4 \left[2\sigma_1^8 n^6 - \sigma_1^4\sigma_2^2 n^4 m^2 (4\sigma_1^2 - 3\sigma_2^2) + \sigma_1^2\sigma_2^4 n^2 m^4 \left(3\sigma_1^2 - 4\sigma_2^2\right) + 2\sigma_2^8 m^6\right]}{3\left(\sigma_1^2 n^2 + \sigma_2^2 m^2\right)^7} + O(1/n^6).$$

The two opposite bond angles, ω_1 and ω_2 are expanded by substituting (12) and (13) into the Eq. 9 for $\cos\omega_1$ and $\cos\omega_2$ to obtain

$$\cos\omega_1 = -1 + \left(2\sigma_1^6 n^4 \pi^2\right) / \left(\sigma_1^2 n^2 + \sigma_2^2 m^2\right)^3 + O(1/n^4),$$
$$\cos\omega_2 = -1 + \left(2\sigma_2^6 m^4 \pi^2\right) / \left(\sigma_1^2 n^2 + \sigma_2^2 m^2\right)^3 + O(1/n^4).$$

The first term is exactly the rolled-up model value and the second term is the first-order correction to the conventional value.

Using the same technique asymptotic expansions may be developed for the nanotube radius r and is given by

$$r = \frac{\sqrt{\sigma_1^2 n^2 + \sigma_2^2 m^2}}{2\pi} + \frac{\pi\left[\sigma_1^8 n^6 + 4\sigma_1^2\sigma_2^2 n^2 m^2\left(\sigma_1^4 n^2 + \sigma_2^4 m^2\right) + \sigma_2^8 m^6\right]}{12\left(\sigma_1^2 n^2 + \sigma_2^2 m^2\right)^{7/2}} + O\left(\frac{1}{n^3}\right), \tag{15}$$

where the leading order term is exactly the conventional expression 5. Similarly, it can be shown that the second term is a first-order correction to the conventional radius which is due to the curvature of the structure, which can be written in terms of the conventional chiral angle θ_0 and the conventional radius r_0 by Eqs. 1 and 5 as

$$r = r_0 + \left[\sigma_1^2 \cos^4\theta_0(4 - 3\cos^2\theta_0) + \sigma_2^2 \sin^4\theta_0(4 - 3\sin^2\theta_0)\right]/(24r_0) + O(1/n^3). \tag{16}$$

An asymptotic expansion of the unit cell length L yields

$$L = \frac{\sqrt{n^2\sigma_2^2 p_\lambda^2 + m^2\sigma_1^2 q_\lambda^2}}{d_R} - \frac{\sigma_1^2\sigma_2^2 n^2 m^2 \pi^2\left(\sigma_1^4 n^2 + \sigma_2^4 m^2\right)\sqrt{n^2\sigma_2^2 p_\lambda^2 + m^2\sigma_1^2 q_\lambda^2}}{2\left(\sigma_1^2 n^2 + \sigma_2^2 m^2\right)^4 d_R} + O\left(\frac{1}{n^3}\right), \tag{17}$$

where we note that the first term in Eq. 17 is exactly the conventional expression 3. It may be shown that the second term is a first-order correction to the conventional unit cell length which is due to the curvature of the structure, which is given by

$$L = L_0 - \left[L_0\left(\sigma_1^2\cos^2\theta_0 + \sigma_2^2\sin^2\theta_0\right)\sin^2(2\theta_0)\right]/(32r_0^2) + O(1/n^3). \tag{18}$$

5 Results

Figure 5 shows that a plot of the radius r_λ divided by σ_1 versus the ratio of bond lengths $\lambda = \sigma_1/\sigma_2$ for $n = 3$ and 4 and various values of m, where r_λ is the radius in the λ ratio system. This figure shows the change in the radius as a function of the bond length σ_2. The prismatic types show a constant variation because the radius of the prismatic type depends only on σ_1. For antiprismatic tubes, the bond lengths have the same contribution to the radius when they are equal and therefore a longer bond length contributes more to increasing the radius. The figure shows that the antiprismatic types have a larger change in curvature because σ_2 decreasing corresponds to λ increasing. In all other cases, the chiral tubes exhibit behavior that is between the prismatic and the antiprismatic tubes.

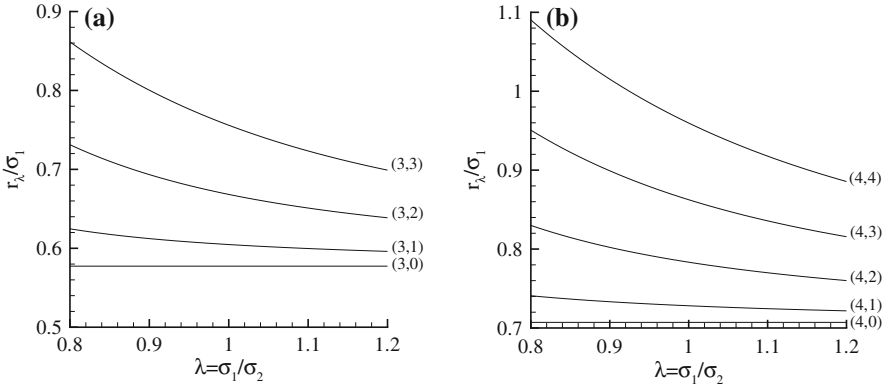

Fig. 5 Variation of r_λ/σ_1 with $\lambda = \sigma_1/\sigma_2$ for $n = 3$ and 4, **a** $(3, m)$ and **b** $(4, m)$

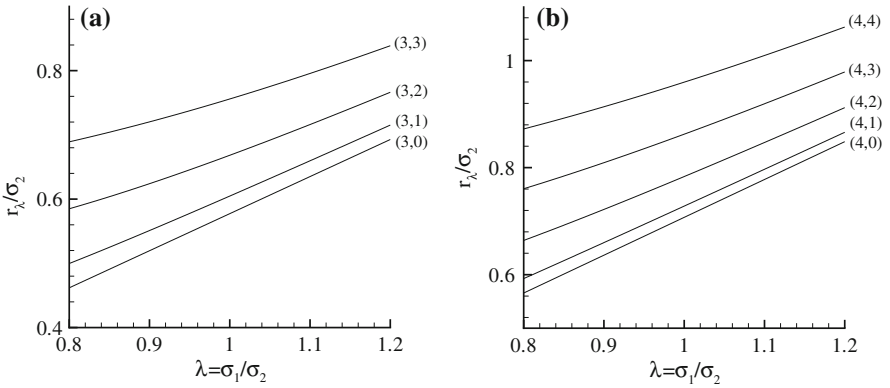

Fig. 6 Variation of r_λ/σ_2 with $\lambda = \sigma_1/\sigma_2$ for $n = 3$ and 4, **a** $(3, m)$ and **b** $(4, m)$

Similarly, Fig. 6 shows the variation of the radius r_λ divided by σ_2 versus the ratio of bond lengths $\lambda = \sigma_1/\sigma_2$ for $n = 3$ and 4 and various values of m. Again, the prismatic types show a straight line because the radii of prismatic tubes depend only on σ_1. Although (3,0) and (4,0) are straight lines, they have different slopes because the radius also depends on n. The figure shows the variation for $(3, m)$ and $(4, m)$ tubes and that the gradient of the lines decrease as m increases.

By examining the asymptotic expansions of the equations for the polyhedral model for the chiral angles (14), the radius (16) and the unit cell length (18), we observe that the leading order term of the analytical expressions gives the conventional formulae as their highest order term and that the second term is a first-order correction to the conventional model. This demonstrates that the polyhedral model converges to the conventional model for large n. The equations for the subtend semi-angle (6), the chiral angles (7), the adjacent bond angle (8), the opposite bond angles (9), the radius (10) and the unit cell length (11) are the same as those given in Lee et al. [17], when the bond lengths are equal. Our polyhedral model for the skew rhombi structure

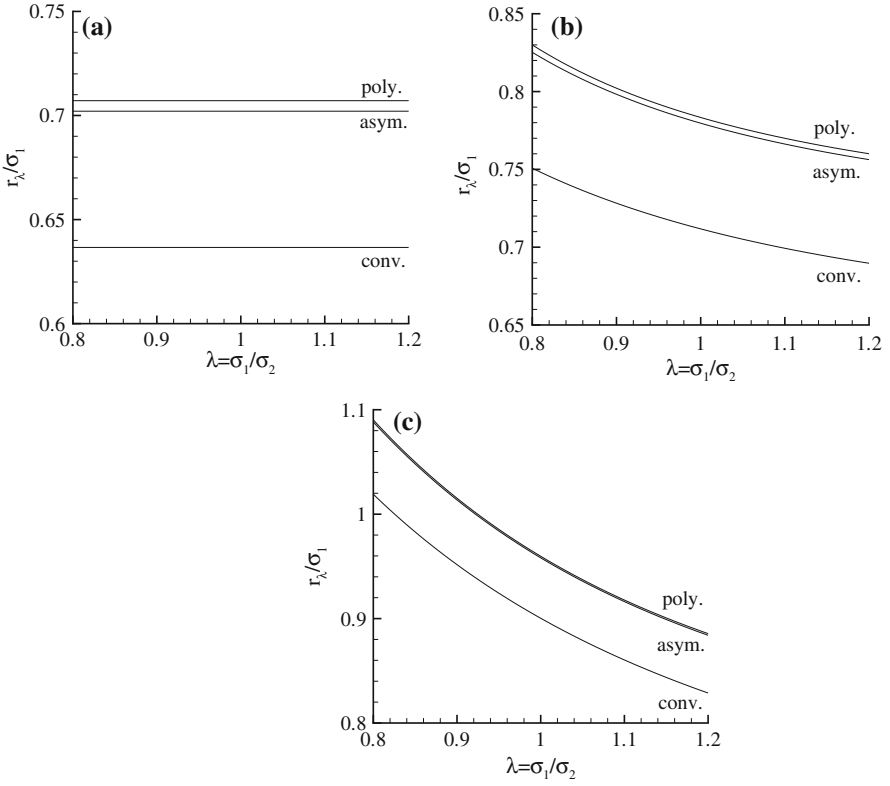

Fig. 7 Comparison of r_λ/σ_1 as a function of $\lambda = \sigma_1/\sigma_2$ for various models (polyhedral, asymptotic, conventional), **a** (4, 0), **b** (4, 2) and **c** (4, 4)

with distinct bond lengths might also be applied to other materials for those nanotubes which are also based on the skew rhombi structure.

Figure 7 shows a plot of the radius r_λ divided by σ_1 versus the ratio of bond lengths $\lambda = \sigma_1/\sigma_2$ for the prismatic, chiral and antiprismatic tubes. The radius of the polyhedral and the conventional models is obtained from the exact formulae (10) and (5), and the radius for the asymptotic expansion is obtained using the first two terms of the expansion (15). We observe that all three models display a similar variation with λ, except that the conventional model is quite different in terms of the absolute magnitude of the predicted radii. The asymptotic expansion is very close to the polyhedral model where the first term of the asymptotic expansion is exactly the conventional expression, and the second term of the asymptotic expansion is a first-order correction to the conventional model. Similarly, Fig. 8 shows a plot of the different models for the radius r_λ divided by σ_2 versus the ratio of bond lengths $\lambda = \sigma_1/\sigma_2$, which are essentially linear in λ for different nanotube types and different models.

To provide some independent numerical data that the structures considered here are at least meta-stable, we have relaxed the idealised silicon nanotube structures with

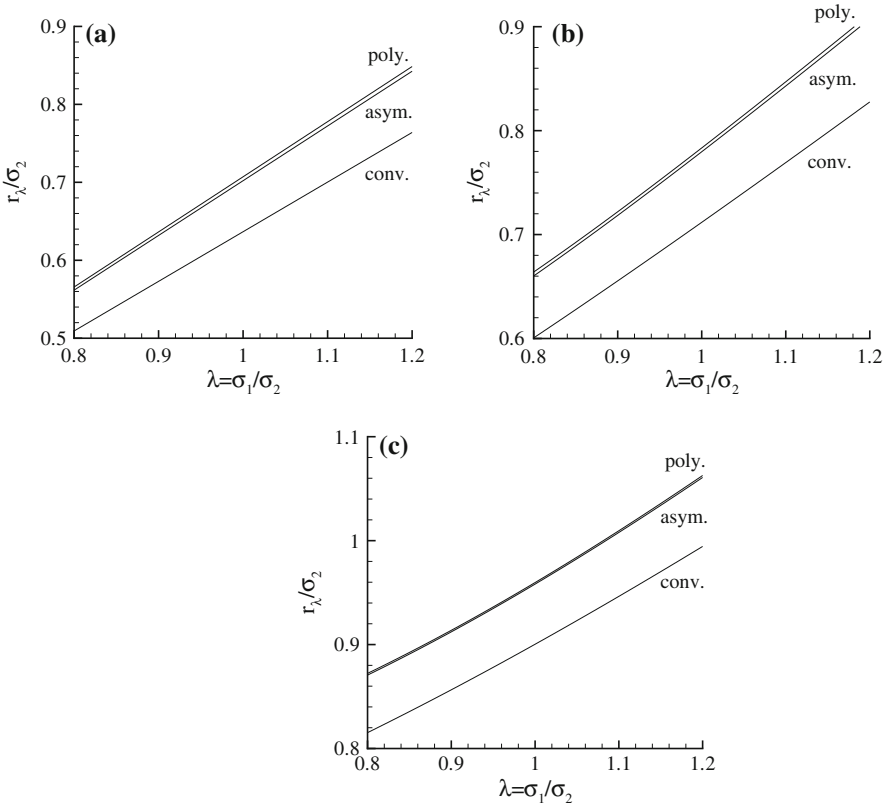

Fig. 8 Comparison of r_λ/σ_2 as a function of $\lambda = \sigma_1/\sigma_2$ for various models (polyhedral, asymptotic, conventional), **a** (4, 0), **b** (4, 2) and **c** (4, 4)

all the bond lengths set equal to 2.35 Å using the LAMMPS software (see Lee et al. [17] and Plimpton [18]) and we model the silicon pairwise interactions using a Stillinger-Weber potential [19]. Our approach is then to establish the simulations for an initial temperature of $\mathcal{T}$ Kelvin with $\mathcal{T} \in \{100, 200, \ldots, 600\}$ which is reduced to zero Kelvin over 100,000 time steps, and at the end of the simulations the structures are examined for inconsistencies. For silicon nanotubes (n, m) with 500 atoms which $n \in \{3, 4, \ldots, 10\}$ and $m \in \{0, 1, \ldots, n\}$, the simulation domain extends 6 nm in both the x and y directions for non-periodic and shrink-wrapped boundary conditions. The length in the z direction is based on a tube comprising 500 atoms and we employ a periodic boundary condition in the z direction.

After the molecular dynamics simulations, most of the silicon nanotubes considered here appear not to stabilize as recognizable tubes and only nine of the silicon nanotubes are found to have a stable tube structure out of originally considering sixty tubes. The nine stable tubes found are (4,0), (5,0), (6,0) and (7,0) for the prismatic type and (4,1), (4,2), (5,1), (6,1) and (7,1) for the chiral type. The simulations indicate that all the antiprismatic types considered are unstable structures. However, all the

Table 1 Results of molecular dynamics simulations for stable silicon nanotubes at 100 K

(n, m)	σ_1^*(Å)	σ_2^*(Å)	r^* (Å)	r (Å)	r_0 (Å)	$\mathcal{T}_{ac}(K)$
(4,0)	2.462 ± 0.031	2.573 ± 0.040	1.74 ± 0.08	1.74	1.57	1,400
(4,1)	2.431 ± 0.032	2.588 ± 0.017	1.75 ± 0.07	1.78	1.60	1,000
(4,2)	2.479 ± 0.023	2.611 ± 0.040	1.88 ± 0.03	1.96	1.78	300
(5,0)	2.418 ± 0.051	2.574 ± 0.038	2.12 ± 0.01	2.06	1.92	1,000
(5,1)	2.413 ± 0.012	2.571 ± 0.021	2.07 ± 0.05	2.10	1.96	800
(6,0)	2.429 ± 0.066	2.580 ± 0.087	2.42 ± 0.07	2.43	2.32	800
(6,1)	2.449 ± 0.055	2.564 ± 0.076	2.47 ± 0.45	2.49	2.37	600
(7,0)	2.466 ± 0.098	2.571 ± 0.091	2.84 ± 0.69	2.84	2.75	500
(7,1)	2.447 ± 0.037	2.602 ± 0.028	2.83 ± 0.43	2.85	2.76	400

stable nanotube structures become unstable when the initial temperature $\mathcal{T}$ Kelvin is increased, and the temperature at which the structure becomes unstable is called the critical temperature. In order to examine the critical temperature for the stable nanotubes, they are simulated again with 100 atoms from 100 to 1,500 K and increasing by 100 K. The critical temperature so obtained is an approximate critical temperature $\mathcal{T}_{ac}$, since the temperature is examined only for every hundred Kelvin. All the initial bond lengths are set to be the same value but after the simulations, two distinct bond lengths emerge and the σ_2^* bond length appears to be longer than the σ_1^* bond length, where the * indicates the molecular dynamics simulations results. The stable silicon nanotubes for the bond lengths σ_1^* and σ_2^* and radius r^* which are measured at 100 K simulations and the radii r, r_0 which are the radius for the polyhedral model and the rolled-up model using σ_1^* and σ_2^* are shown in Table 1 and the adjacent bond angle ϕ^* and ϕ and the opposite bond angles ω_1^*, ω_2^*, ω_1 and ω_2 are shown in Table 2. The bond lengths σ_1^* and σ_2^* and the radii r^*, r and r_0 for (4, 0) at different temperatures are shown in Table 3. The actual nanotubes obtained from the molecular dynamics simulations for (4, 0), (4, 1) and (4, 2) are shown in Figs. 9, 10 and 11.

Table 1 shows a comparison of the radius for the polyhedral model and the rolled-up model with distinct bond lengths as compared with the molecular dynamics simulations at 100 K and it is apparent that the results of the polyhedral model and the molecular dynamics simulations are in excellent agreement. However, there is a large difference for the radius predicted by the rolled-up model and that for the molecular dynamics simulations, especially for the smaller radii nanotubes. The approximate critical temperatures $\mathcal{T}_{ac}$ show that the prismatic $(n, 0)$ tubes and the $(n, 1)$ chiral tubes are stable structures for $n \in \{4, 5, 6, 7\}$. For $(n, 2)$ chiral, only (4, 2) provides a possible stable tube structure. The other chiral and all the antiprismatic tubes apparently could not be formed and therefore they may be unstable structures. The structure of the nanotube becomes increasingly unstable as both m and n increase. Thus, the approximate critical temperatures $\mathcal{T}_{ac}$ decrease when n or m increase. As a result, the ultra-small and very large radii nanotubes tend not to occur, and there is a definite range of radii found from the molecular dynamics simulations ($1.74\text{Å} \leq r \leq 2.83\text{Å}$).

Table 2 shows a comparison of the bond angles for the polyhedral model with distinct bond lengths as compared with the molecular dynamics simulations at 100 K.

Table 2 Results of bond angles from molecular dynamics simulations for stable silicon nanotubes at 100 K

(n, m)	$\phi^*(^\circ)$	$\phi_a^*(^\circ)$	$\phi_b^*(^\circ)$	$\omega_1^*(^\circ)$	$\omega_2^*(^\circ)$	$\phi(^\circ)$	$\omega_1(^\circ)$	$\omega_2(^\circ)$
(4,0)	90.13 ± 15.69	82.57 ± 1.72	97.68 ± 1.34	90.00 ± 5.21	158.08 ± 2.40	90.00	90.00	180.00
(4,1)	88.49 ± 10.82	83.27 ± 0.87	93.71 ± 0.99	98.63 ± 0.56	174.79 ± 1.34	86.98	100.27	170.59
(4,2)	85.58 ± 12.83	79.39 ± 0.97	91.78 ± 1.01	118.03 ± 1.31	162.86 ± 3.04	84.34	119.02	157.60
(5,0)	89.99 ± 12.08	84.70 ± 5.30	95.29 ± 5.54	107.99 ± 2.15	162.30 ± 2.04	90.00	108.00	180.00
(5,1)	89.40 ± 8.37	85.37 ± 1.18	93.44 ± 1.29	112.12 ± 1.08	178.13 ± 1.20	88.79	113.19	175.61
(6,0)	89.98 ± 13.58	83.94 ± 5.69	96.02 ± 5.90	119.94 ± 4.90	160.33 ± 4.69	90.00	120.00	180.00
(6,1)	89.46 ± 14.81	82.49 ± 4.85	96.43 ± 3.41	112.43 ± 11.90	158.94 ± 8.96	89.46	122.87	177.73
(7,0)	89.93 ± 18.04	81.59 ± 5.65	98.26 ± 6.67	128.39 ± 10.76	152.97 ± 8.32	90.00	128.57	180.00
(7,1)	89.52 ± 12.95	83.68 ± 5.42	95.36 ± 5.03	130.32 ± 8.49	160.01 ± 7.15	89.70	130.41	178.57

Table 3 Results of molecular dynamics simulations for (4, 0) at different temperatures

$\mathcal{T}$ (K)	σ_1^* (Å)	σ_2^* (Å)	r^* (Å)	r (Å)	r_0 (Å)
100	2.462 ± 0.031	2.573 ± 0.040	1.74 ± 0.08	1.74	1.57
200	2.462 ± 0.022	2.573 ± 0.040	1.74 ± 0.08	1.74	1.57
300	2.445 ± 0.016	2.595 ± 0.018	1.73 ± 0.04	1.73	1.56
400	2.454 ± 0.031	2.592 ± 0.072	1.73 ± 0.05	1.74	1.56
500	2.450 ± 0.047	2.588 ± 0.041	1.73 ± 0.05	1.73	1.56
600	2.439 ± 0.020	2.588 ± 0.038	1.73 ± 0.05	1.72	1.55
700	2.451 ± 0.030	2.587 ± 0.026	1.73 ± 0.05	1.73	1.56
800	2.448 ± 0.031	2.585 ± 0.052	1.73 ± 0.03	1.73	1.56
900	2.446 ± 0.029	2.597 ± 0.037	1.73 ± 0.04	1.73	1.56
1,000	2.443 ± 0.018	2.590 ± 0.023	1.73 ± 0.04	1.73	1.56

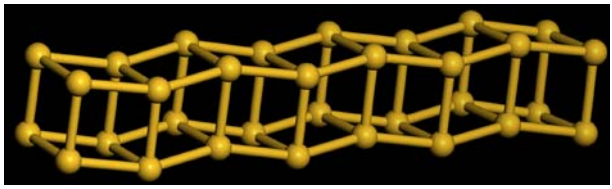

Fig. 9 (4, 0) at 100 K

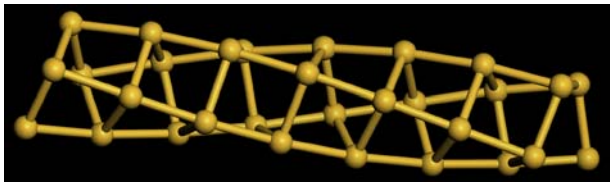

Fig. 10 (4, 1) at 100 K

The bond angles ϕ^*, ω_1^* and ω_2^* are the average of the bond angles measured from two rings of the nanotube and the error is two standard deviations. The bond angles ϕ, ω_1 and ω_2 are calculated from the polyhedral model using the values σ_1^* and σ_2^*. The results of the adjacent bond angle ϕ and the opposite bond angle ω_1 of the polyhedral model and the molecular dynamics simulations are in excellent agreement. The calculated adjacent bond angle ϕ^* has a large error, and therefore we have grouped the raw data into two groups as either above or below 90° which are termed the adjacent bond angles ϕ_a^* and ϕ_b^*. The low value of the error obtained for the adjacent bond angles ϕ_a^* and ϕ_b^* suggests that the adjacent bond angle may have two distinct values. The opposite bond angle ω_2 for prismatic tubes does not match well with the molecular dynamics simulations results because the tube possesses an off-centred structure which alternates along the nanotube length as shown in Fig. 9. The structures of the molecular dynamics simulations results for (4,1) and (4,2) which are shown in Figs. 10 and 11 are similar to those predicted from the polyhedral model.

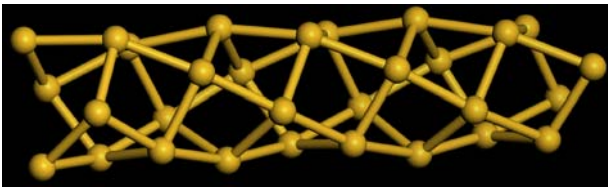

Fig. 11 (4, 2) at 100 K

6 Conclusion

Silicon nanotubes are formed from stable structures by sp^3 bond hybridization which leads to four coordinated atoms that adopt a skew rhombic lattice, so that they may have different bond lengths in different directions [9]. The main geometric parameters are shown in Table 4 for the conventional rolled-up model. By formulating the polyhedral model which is based on the three fundamental postulates, which are that all the bond lengths lying on the same helix are equal, that all the adjacent bond angles are equal and that all atomic nuclei are equidistant from a common axis, we have derived equations for the key geometric parameters that arise, such as the subtend angle 2ψ, the chiral angles θ_1 and θ_2, the adjacent bond angle ϕ, the opposite bond angles ω_1 and ω_2, the radius r and the unit cell length L (see Table 5). The subtend semi-angle ψ is the fundamental variable on which all the other parameters depend and we find that it is determined from the transcendental Eq. 6 and therefore cannot be written as a simple analytical function of λ, n and m. The radius r as given by Eq. 10 is a homogeneous function of degree one in σ_1 and σ_2. We see from Fig. 6 that r_λ/σ_2 is essentially linear in $\lambda = \sigma_1/\sigma_2$. Figures 7 and 8 demonstrate that the first two terms of the asymptotic expansion (15) constitute a very accurate approximate formula for the radius r as given by (10). It is also apparent from these figures that there are significant differences between the conventional rolled-up model and the polyhedral model. The polyhedral model converges to the conventional model for large n because the leading term of the analytical expressions gives the conventional formulae as the highest order term, while the second order term may be viewed as a first-order correction to

Table 4 Main equations for rolled-up model

Parameter name	Equation
Chiral vector $\mathbf{C_h}$	$\mathbf{C_h} = n\mathbf{a_1} + m\mathbf{a_2}$
Conventional translational vector $\mathbf{T_0}$	$\mathbf{T_0} = (-m\mathbf{a_1})/d_{0R} + (n\mathbf{a_2})/d_{0R}$
New translational vector $\mathbf{T}$	$\mathbf{T} = (-mq_\lambda\mathbf{a_1})/d_R + (np_\lambda\mathbf{a_2})/d_R$
Chiral angle θ_0	$\cos^2\theta_0 = \left(\sigma_1^2 n^2\right) / \left(\sigma_1^2 n^2 + \sigma_2^2 m^2\right)$
Conjugate chiral angle $\bar{\theta_0}$	$\cos^2\bar{\theta_0} = \left(\sigma_2^2 m^2\right) / \left(\sigma_1^2 n^2 + \sigma_2^2 m^2\right)$
Unit cell length L_0	$L_0 = \sqrt{\sigma_2^2 n^2 p_\lambda^2 + \sigma_1^2 m^2 q_\lambda^2}/d_R$
Number of atoms in the unit cell N	$N = (n^2 p_\lambda + m^2 q_\lambda)/d_R$
Nanotube radius r_0	$r_0 = \sqrt{\sigma_1^2 n^2 + \sigma_2^2 m^2}/(2\pi)$

Table 5 Main equations for polyhedral model $\lambda = \sigma_1/\sigma_2$

Parameter name	Equation
Subtend semi-angle ψ	$4nm(\sin^2\psi - \lambda^2\sin^2\xi) + (\lambda^2 n^2 - m^2)[\sin^2(\xi+\psi) - \sin^2(\xi-\psi)] = 0$
Chiral angle θ_1	$\cos^2\theta_1 = \dfrac{n\sin\psi}{n\sin\psi - m\cos\psi\sin\xi\cos\xi}$
Conjugate chiral angle θ_2	$\cos^2\theta_2 = \dfrac{m\sin\xi}{m\sin\xi - n\sin\psi\cos\psi\cos\xi}$
Adjacent bond angle ϕ	$\cos\phi = \dfrac{(\lambda^2+1)m^2\sin^2\psi - \lambda^2 m^2\cos^2\theta_1\sin^2(\xi+\psi) - \lambda^2(n+m)^2\sin^2\theta_1\sin^2\psi}{2m^2\lambda\sin^2\psi}$
Opposite bond angle ω_1	$\cos\omega_1 = 2\cos^2\theta_1\sin^2\psi - 1$
Opposite bond angle ω_2	$\cos\omega_2 = 1 - \dfrac{2\lambda^2 n^2\sin^2\theta_1}{m^2} - \dfrac{\lambda^2\cos^2\theta_1\sin^2 2\xi}{2\sin^2\psi}$
Nanotube radius r	$r = \dfrac{\sigma_1\cos\theta_1}{2\sin\psi}$
Number of atoms in the unit cell N	$N = \dfrac{n^2 p_\lambda + m^2 q_\lambda}{d_R}$
Unit cell length L	$L = \dfrac{\sigma_1(n^2 p_\lambda + m^2 q_\lambda)\sin\theta_1}{m d_R}$

the conventional model. The polyhedral model with distinct bond lengths includes all the results for the polyhedral model with equal bond lengths [17].

From the molecular dynamics simulations, only nine silicon nanotubes appear to have a stable tube structure out of originally considering sixty possible tubes. The tubes found to be stable are (4,0), (5,0), (6,0) and (7,0) for the prismatic and (4,1), (4,2), (5,1), (6,1) and (7,1) for the chiral. The antiprismatic and most of the chiral tubes appear to be unstable structures. The approximate critical temperatures $\mathcal{T}_{ac}$ are shown to decrease with increasing m and n, and the ultra-small and very large radii nanotubes tend not to occur, and there is a definite range of radii found from the molecular dynamics simulations ($1.74\text{Å} \leq r \leq 2.83\text{Å}$). Comparisons of the radii for the stable nanotubes with the molecular dynamics simulations show that the radii predicted by the polyhedral model with distinct bond lengths are in excellent agreement. The adjacent bond angle ϕ and the opposite bond angle ω_1 of the polyhedral model and the molecular dynamics simulations are also in excellent agreement. The adjacent bond angle ϕ^* appears to have two distinct values ϕ_a^* and ϕ_b^* because the error of the actual ϕ^* is very large as compared with the relatively small errors of ϕ_a^* and ϕ_b^*. The opposite bond angle ω_2 for prismatic tubes does not match with the molecular dynamics simulations results because the simulated tubes adopt an alternating off-centred structure. However, the structures of the molecular dynamics simulations results for (4, 1) and (4, 2) coincide with the polyhedral model.

Acknowledgments The support of the Australian Research Council, both through the Discovery Project Scheme and for providing an Australian Professorial Fellowship for JMH and an Australian Post-doctoral Fellowship for BJC is gratefully acknowledged.

Appendix A: Asymptotic expansions of exact formulae

The root of the subtend semi-angle ψ in (6) is determined by a series expansion in powers of $1/n$ and we then use this as the basis for determining series expansions for all of the other parameters derived in the previous section. Firstly, (6) is written in the form

$$4h\left(\sigma_2^2\sin^2\psi-\sigma_1^2\sin^2\xi\right)+\left(\sigma_1^2-\sigma_2^2h^2\right)\left[\sin^2(\xi+\psi)-\sin^2(\xi-\psi)\right]=0, \quad (19)$$

where $\xi=(\psi-\pi/n)/h$ and $h=m/n$. The numbers m and n are assumed to be of the same magnitude, so that the order of h is assumed to be of order one. As n increases ψ becomes small, and therefore (19) can be expanded in terms of ψ and $1/n$, where we define the series as

$$\psi=\frac{\psi_0(h)}{n}+\frac{\psi_1(h)}{n^3}+\frac{\psi_2(h)}{n^5}+\cdots,$$
$$\cos^2\theta_1=a_0(h)+\frac{a_1(h)}{n^2}+\frac{a_2(h)}{n^4}+\cdots.$$

By the method of asymptotic expansions we may derive

$$\psi_0(h) = \frac{\sigma_1^2 \pi}{\sigma_1^2 + \sigma_2^2 h^2}, \quad \psi_1(h) = -\frac{\sigma_1^2 \sigma_2^2 h^2 \pi^3 \left[\sigma_1^6 - 2\sigma_1^2 \sigma_2^2 h^2 (\sigma_1^2 - \sigma_2^2) - \sigma_2^6 h^4\right]}{3\left(\sigma_1^2 + \sigma_2^2 h^2\right)^5}, \tag{20}$$

which gives ψ is in its asymptotic form (12), by substituting for $h = m/n$ in (20).

Now the equation for $\cos^2 \theta_1$ (7) is expanded by substituting the asymptotic expansion for ψ. As a result, we find that the expansion coefficients are given by

$$a_0(h) = \frac{\sigma_1^2}{\sigma_1^2 + \sigma_2^2 h^2}, \quad a_1(h) = \frac{\sigma_1^2 \sigma_2^4 \pi^2 h^4 \left(\sigma_1^4 + \sigma_2^4 h^2\right)}{\left(\sigma_1^2 + \sigma_2^2 h^2\right)^5}.$$

Similarly, the asymptotic equation of the conjugate chiral angle $\cos^2 \theta_2$ (7) is expressed as

$$\cos^2 \theta_2 = \frac{\sigma_2^2 h^2}{\sigma_1^2 + \sigma_2^2 h^2} + \frac{\sigma_1^4 \sigma_2^2 \pi^2 h^2 \left(\sigma_1^4 + \sigma_2^4 h^2\right)}{\left(\sigma_1^2 + \sigma_2^2 h^2\right)^5} \frac{1}{n^2} + O\left(\frac{1}{n^4}\right).$$

The adjacent bond angle ϕ is found from substituting the asymptotic equation of ψ in (8) which is given by

$$\begin{aligned} \cos \phi = & \frac{\sigma_1^3 \sigma_2^3 h^2 \pi^2}{(\sigma_1^2 + \sigma_2^2 h^2)^3} \frac{1}{n^2} \\ & + \frac{\sigma_1^3 \sigma_2^3 h^2 \pi^4 \left[2\sigma_1^8 - \sigma_1^4 \sigma_2^2 h^2 \left(4\sigma_1^2 - 3\sigma_2^2\right) + \sigma_1^2 \sigma_2^4 h^4 \left(3\sigma_1^2 - 4\sigma_2^2\right) + 2\sigma_2^8 h^6\right]}{3\left(\sigma_1^2 + \sigma_2^2 h^2\right)^7} \frac{1}{n^4} \\ & + O(1/n^6). \end{aligned}$$

The series expansion of the opposite bond angle ω_1 is found by substituting the series expansion for $\cos^2 \theta_1$ and expanding the asymptotic equation for ψ. As a result, $\cos \omega_1$ is given by

$$\cos \omega_1 = -1 + 2C^2 \psi^2 - (2C^2 \psi^4)/3 + O(\psi^6),$$

where $C = \cos \theta_1$. The asymptotic expansion of the opposite bond angle ω_2 is obtained by substituting the series expansions for ψ and $\cos \theta_1$ given by

$$\cos \omega_2 = -1 + \frac{2\sigma_2^6 h^4 \pi^2}{\left(\sigma_1^2 + \sigma_2^2 h^2\right)^3} \frac{1}{n^2} + O\left(\frac{1}{n^4}\right).$$

By substitution of the series expansion for $\cos\theta_1$ into the formula for the nanotube radius (10), and then expanding as a series in powers of ψ, we derive

$$r = (\sigma_1 C)/(2\psi) + (\sigma_1 C\psi)/12 + O(\psi^3), \tag{21}$$

The unit cell length L (11) can be expressed by the following expansion

$$L = \frac{\sqrt{\sigma_2^2 p_\lambda^2 + h^2\sigma_1^2 q_\lambda^2}}{d_R} n - \frac{\sigma_1^2\sigma_2^2 h^2\pi^2(\sigma_1^4 + \sigma_2^4 h^2)\sqrt{\sigma_2^2 p_\lambda^2 + h^2\sigma_1^2 q_\lambda^2}}{2(\sigma_1^2 + \sigma_2^2 h^2)^4 d_R}\frac{1}{n} + O\left(\frac{1}{n^3}\right). \tag{22}$$

where $C = \cos\theta_1$. From (21), (22) and the series expansions (12) and (13) for ψ and $C = \cos\theta_1$, we may produce expansions for the nanotube radius r and unit cell length L, which is given by (15) and (17), respectively.

References

1. S. Iijima, Nature **354**(6348), 56 (1991)
2. S.Y. Jeong, J.Y. Kim, H.D. Yang, B.N. Yoon, S.H. Choi, H.K. Kang, C.W. Yang, Y.H. Lee, Adv. Mater. **15**(14), 1172 (2003)
3. J. Sha, J. Niu, X. Ma, J. Xu, X. Zhang, Q. Yang, D. Yang, Adv. Mater. **14**(17), 1219 (2002)
4. B.X. Li, P.L. Cao, J. Mol. Struct. (TheoChem) **679**, 127–130 (2004)
5. R.Q. Zhang, S.T. Lee, C.K. Law, W.K. Li, B.K. Teo, Chem. Phys. Lett. **364**, 251–258 (2002)
6. E. Durgun, S. Tongay, S. Ciraci, Phys. Rev. B **72**, 075420 (2005)
7. D.F. Perepichka, F. Rosei, Small **2**(1), 22–25 (2006)
8. X. Wang, Z. Huang, T. Wang, Y.W. Tang, X.C. Zeng, Physica B **403**, 2021–2028 (2008)
9. J. Bai, X.C. Zeng, H. Tanaka, J.Y. Zeng, Proc. Natl. Acad. Sci. **101**(9), 2664–2668 (2004)
10. M.S. Dresselhaus, G. Dresselhaus, R. Saito, Phys. Rev. B **45**(11), 6234–6242 (1992)
11. M.S. Dresselhaus, G. Dresselhaus, R. Saito, Carbon **33**(7), 883–891 (1995)
12. R.A. Jishi, M.S. Dresselhaus, G. Dresselhaus, Phys. Rev. B **47**(24), 16671 (1993)
13. A. Gindulyte, W.N. Lipscomb, L. Massa, Inorg. Chem. **37**(25), 6544–6545 (1998)
14. V. Dadashev, A. Gindulyte, W.N. Lipscomb, L. Massa, R. Squire, in *Structures and Mechanisms: From Ashes to Enzymes*, Chap. 5 ed. by G.R. Eaton, D.C. Wiley, O. Jardetzky (Oxford University Press, Washington, 2002), pp.79–102
15. B.J. Cox, J.M. Hill, Carbon **45**, 1453–1462 (2007)
16. B.J. Cox, J.M. Hill, Carbon **46**, 711–713 (2008)
17. R.K.F. Lee, B.J. Cox, J.M. Hill, J. Phys. Condens. Matter **21**, 075301 (2008)
18. S.J. Plimpton, J. Comput. Phys. **117**, 1–19 (1995)
19. F.H. Stillinger, T.A. Weber, Phys. Rev. B **31**, 5262–5271 (1985)